# Effects of Fling Step and Forward Directivity on Seismic Response of Buildings

**Erol Kalkan,**[a] **S.M.EERI, and Sashi K. Kunnath,**[a] **M.EERI**

This paper investigates the consequences of well-known characteristics of near-fault ground motions on the seismic response of steel moment frames. Additionally, idealized pulses are utilized in a separate study to gain further insight into the effects of high-amplitude pulses on structural demands. Simple input pulses were also synthesized to simulate artificial fling-step effects in ground motions originally having forward directivity. Findings from the study reveal that median maximum demands and the dispersion in the peak values were higher for near-fault records than far-fault motions. The arrival of the velocity pulse in a near-fault record causes the structure to dissipate considerable input energy in relatively few plastic cycles, whereas cumulative effects from increased cyclic demands are more pronounced in far-fault records. For pulse-type input, the maximum demand is a function of the ratio of the pulse period to the fundamental period of the structure. Records with fling effects were found to excite systems primarily in their fundamental mode while waveforms with forward directivity in the absence of fling caused higher modes to be activated. It is concluded that the acceleration and velocity spectra, when examined collectively, can be utilized to reasonably assess the damage potential of near-fault records. [DOI: 10.1193/1.2192560]

## INTRODUCTION

In the proximity of an active fault system, ground motions are significantly affected by the faulting mechanism, direction of rupture propagation relative to the site (e.g., forward directivity), as well as the possible static deformation of the ground surface associated with fling-step effects. These near-source outcomes cause most of the seismic energy from the rupture to arrive in a single coherent long-period pulse of motion (note that backward-directivity records typically do not exhibit pulse-type motions). Ground motions having such a distinct pulse-like character arise in general at the beginning of the seismogram, and their effects tend to increase the long-period portion of the acceleration response spectrum (Galesorkhi and Gouchon 2000). These types of ground motions may generate high demands that force the structures to dissipate this input energy with few large displacement excursions. Consequently, the risk of brittle failure for poorly detailed systems is considerably enhanced (Manfredi et al. 2000). The detrimental effects of such phenomena have been recognized during many worldwide earth-

[a] University of California Davis, Department of Civil and Environmental Engineering, Davis, CA 95616



*Earthquake Spectra,* Volume 22, No. 2, pages 367–390, May 2006; 

quakes, including the 1992 Erzincan, 1992 Landers, 1994 Northridge, 1995 Kobe, and most recently the 1999 Kocaeli, Düzce, and Chi-Chi earthquakes.

In contrast to post-earthquake observations, current seismic design practice, based on response spectrum concepts to specify design ground motion, does not by itself provide an adequate representation of near-fault ground motions. This phenomenon is more important for long period buildings. Although recommended and regulatory design codes and provisions such as *ATC-40* (1996), *UBC* (ICBO 1997), *FEMA-356* (ASCE 2000), and *IBC* (ICBO 2000) introduce site-source and distance-dependent near-source factors ($N_A$ and $N_V$) to amplify the elastic design spectrum (i.e., scaling the design base shear), the effectiveness of constant amplification factors in providing adequate ductility levels to structures and components located in the proximity of fault-zones is questionable. This concern arises from the fact that current design spectra were developed using stochastic processes having relatively long duration that characterizes more distant ground motions. Therefore, the pertinent question becomes how vulnerable is the existing building stock to near-fault ground motions, since they were designed accounting primarily for far-fault ground motions. Studies show that high-velocity pulses can place severe inelastic demands on multistory structures (Hall et al. 1995, Heaton et al. 1995). Most recently, Alavi and Krawinkler (2004) demonstrated that intermediate period structures can also be susceptible.

Failures of modern engineered structures observed within the near-fault region in 1994 Northridge earthquake revealed the vulnerability of existing steel buildings against pulse-type ground motions. Additionally, strong directivity effects during the 1999 Kocaeli, Duzce, and Chi-Chi earthquakes renewed attention on the consequences of near-fault ground motions on structures. The objective of this paper, therefore, is to examine the response of typical existing buildings to near-fault ground motions. In the first part of the paper, intrinsic characteristics of near-fault ground motions are reiterated from our current understanding of these events. Three existing steel buildings (of which two were instrumented by the California Strong Motion Instrumentation Program) selected for the evaluation study are then introduced. In order to facilitate an assessment of the effects of near-fault records on structural response, a set of near-fault ground motions having forward directivity and fling step are assembled. These records are used in nonlinear time-history (NTH) analyses, and their results are compared to the response of buildings to typical far-fault ground motions. A perceptive comparison of component demands, story demands, and global system demands for different type of ground motion recordings is presented.

The effect of the ratio of pulse period to the fundamental period of the structure on the inelastic seismic demands of the buildings is also studied. Toward this objective, simple sinusoidal waveforms that adequately describe the nature of pulse-like motions are utilized as seismic input. Additionally, artificial fling-step effects are synthesized into typical near-fault motions having forward directivity, and the structural response of the same buildings is reexamined. Finally, a discussion pertaining to the implication of near-fault ground motions on the design and assessment of structures (and steel moment

frames in particular) is presented. This work is an attempt to collate analytical evidence from nonlinear dynamic analyses on possible structural effects of strong velocity pulses contained in near-fault ground motions.

## CHARACTERISTICS OF NEAR-FAULT GROUND MOTIONS

Far-fault ground motions have been observed as differing dramatically from their near-fault counterparts recorded within a few kilometers of the fault rupture plane. The response of structures to near-fault ground motions can be categorized into two distinct displacement history patterns that depend on the rupture process and corresponding directivity effect. When the rupture propagates forward toward the site, and the direction of slip on the fault is aligned with the site, ground motions oriented in this forward-directivity path may follow certain radiation patterns and generate long-period, short-duration, and large-amplitude pulses (Somerville 1998). Forward directivity occurs where the fault rupture propagates with a velocity close to the shear-wave velocity. Displacement associated with such a shear-wave velocity is largest in the fault-normal direction for strike-slip faults. Records may also exhibit backward directivity, yet they are typically less severe, and do not have distinctive velocity pulses (Somerville et al. 1997a).

On the other hand, fling step, being a result of the evolution of residual ground displacement due to tectonic deformation associated with rupture mechanism, is generally characterized by a unidirectional large-amplitude velocity pulse and a monotonic step in the displacement time history. Fling step occurs in the direction of fault slip and therefore is not strongly coupled with the forward directivity (Abrahamson 2001). It arises in strike-slip faults in the strike parallel direction as in the Kocaeli and Duzce earthquakes (Kalkan et al. 2004), or in the strike-normal direction for dip-slips faults as in the Chi-Chi earthquake (Mavroeidis and Papageorgiou 2003).

Large displacements (permanent ground deformations in the case of fling motion) would be of little consequence if they happen slowly, unless a structure straddled the fault (Hall et al. 1995). However, the duration of these displacements is closely related to the characteristic slip time of a point on the fault, and there is evidence that this slip is rapid (Heaton 1990). Therefore, both shear-wave displacements as in forward directivity, and static displacements as in fling step emerge as pulses. Even for moderate magnitude earthquakes, amplitude of near-fault ground accelerations, velocities, and displacements can be quite high especially in the records having forward directivity. Peak accelerations may exceed 1.0 g, while peak velocities may exceed 2.0 m/sec, and peak displacements can go beyond 2.0 m. The velocity and displacement time histories of typical near-fault ground motions having forward-directivity (Rinaldi record of 1994 Northridge earthquake) and fling-step (Sakarya—SKR record of 1999 Kocaeli earthquake) effects are compared to that of ordinary far-fault motion (Taft record of 1952 Kern County earthquake) in Figure 1. High-velocity pulses are quite distinctive for Rinaldi and SKR records; such pulses do not exist in a typical far-fault ground motion like Taft. The fault-parallel component of the ground motion recorded at SKR station exhibits apparent tectonic deformation at the end of the displacement time history that is a typical signature of fling step.

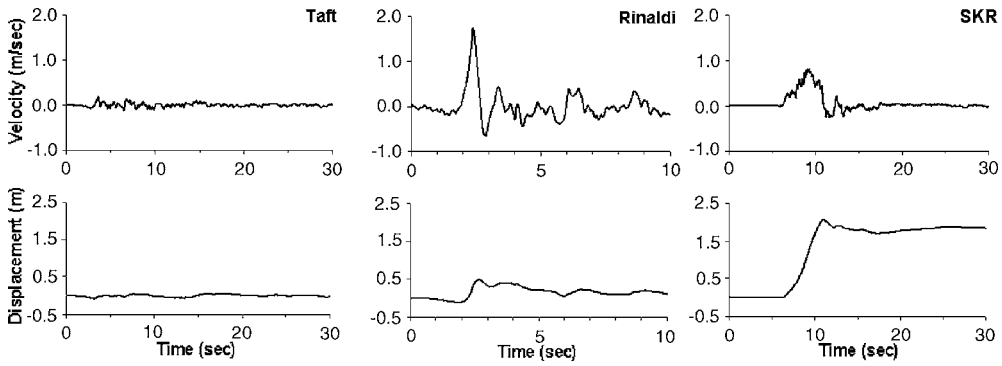


**Figure 1.** Typical velocity and displacement time histories of (a) far-fault, (b) near-fault (forward-directivity), and (c) near-fault (fling-step) ground motions.

## DESCRIPTION OF BUILDINGS USED FOR EVALUATION

Three existing steel special moment-resisting frame (SMRF) buildings were selected as representative case studies to evaluate their seismic demands when subjected to near-fault ground motions with forward directivity and fling step, and to compare and contrast the respective responses to typical far-fault ground motions.

### 4-STORY BUILDING

This building located in Southern California was designed in compliance with the *Uniform Building Code* (*UBC*) (ICBO 1988) specifications. The structural system is composed of perimeter SMRFs to resist lateral loads and interior gravity frames. The floor plan and elevation view of the building with beam and column sections are shown in Figure 2. The columns are embedded into grade beams and anchored to the top of the pile cap, essentially restraining displacements and rotations in all directions. All columns

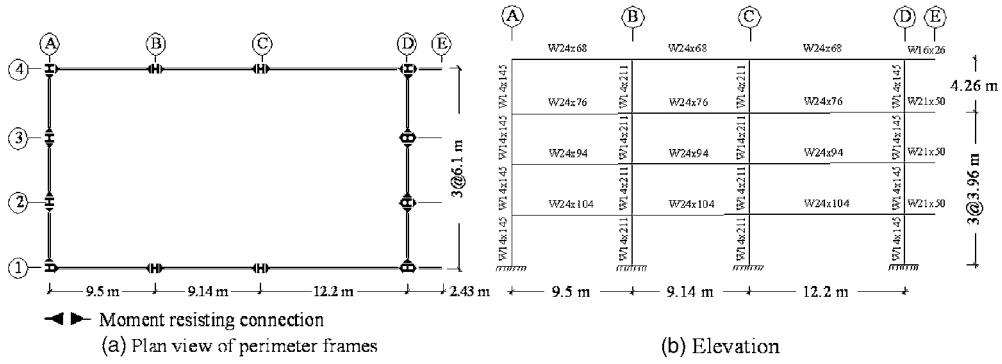


**Figure 2.** Structural configuration of 4-story building.

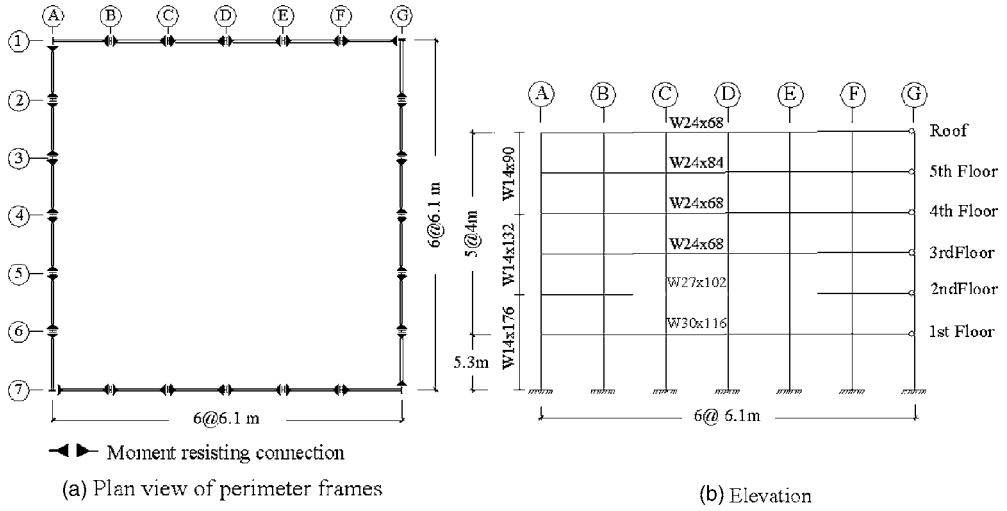


**Figure 3.** Structural configuration of 6-story building.

are made of A-572 grade 50 steel. The girders and beams are made of A-36 steel. The floor system is composed of 15.9-cm-thick slab (8.3-cm lightweight concrete and 7.6-cm composite metal deck) at all floor levels and the roof. The total seismic weight of the building is 10,881 kN. Further details of the building are given in Krawinkler and Al-Ali (1996).

## 6-STORY BUILDING

This moment-frame steel structure was designed in accordance with *UBC* (ICBO 1973) requirements, and is located in Burbank, California. The rectangular plan of the building measures 36.6 m × 36.6 m with a 8.2-cm-thick lightweight concrete slab over 7.5 cm metal decking. The primary lateral load–resisting system is a moment frame around the perimeter of the building. Interior frames are designed to carry only gravity loads. The plan view and the elevation of a typical perimeter frame are shown in Figure 3. The building was instrumented with a total of 13 strong motion sensors at the ground, second, third, and roof levels. All columns are supported by base plates anchored on foundation beams, which in turn are supported on a pair of 9.75 m − 0.75 m diameter concrete piles. Section properties were computed for A-36 steel with an assumed yield stress of 303 MPa. The total building weight (excluding live loads) was estimated to be approximately 34,644 kN.

## 13-STORY BUILDING

This building is located in South San Fernando Valley about 5 km southwest of the Northridge epicenter, and is composed of one basement floor and 13 floors above ground. Built in accordance with the 1973 *UBC*, this structure has been the subject of previous investigations (Kunnath et al. 2004, Uang et al. 1997). As shown in Figure 4, it

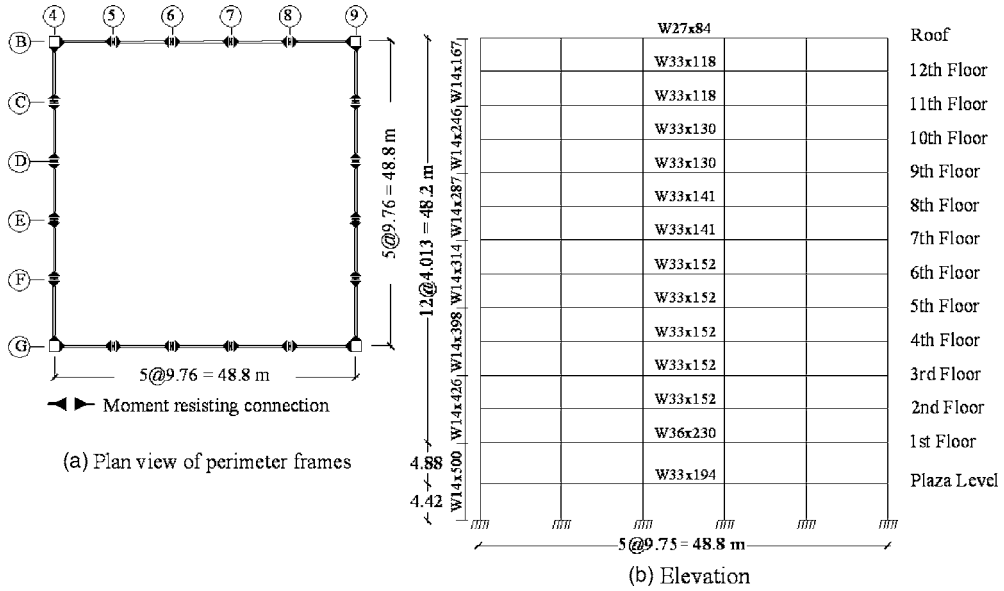


**Figure 4.** Structural configuration of 13-story building.

has a 48.8-m-square plan and an elevation of 57.5 m. The lateral load-resisting system is composed of four identical perimeter frames. The floor plan increases at the second floor to form a plaza level that terminates on three sides into the hillside. The resulting restraint at this level has not been accounted for in this study since the objective of the evaluation is to obtain generic information on moment frames rather than quantify the response of a particular structure. A seismic weight of 140,909 kN was used in the evaluation of this structure.

## DEVELOPMENT OF ANALYTICAL MODELS

The nonlinear evaluations were carried out using a typical two-dimensional frame from each of the buildings. The computer simulations were carried out using the open-source finite-element platform, OpenSees (2005). A force-based nonlinear beam-column element that utilizes a layered "fiber" section is utilized to model all components of the frame models. A fiber section model at each integration point, which in turn is associated with uniaxial material models and enforces Bernoulli beam assumptions for axial force and bending, represents the force-based element. Centerline dimensions were used in the element modeling for all cases. For the time-history evaluations, one half of the total building mass was applied to the frame distributed proportionally to the floor nodes.

Since our objective is not to evaluate the seismic performance of these particular buildings but to utilize typical moment frames of varying height, the simulation of special features such as local connection fracture is not the primary concern. Consequently,

the modeling of the members and connections was based on the assumption of stable hysteresis derived from a bilinear stress-strain model. In constructing the computer models, the columns were assumed to be fixed at the base level. In the case of the 4-story building, the exterior frame along Line-1 was modeled. Similarly, frame models for the 6- and 13-story buildings were developed along Line-1 and Line-G, respectively. Additional details of the 6- and 13-story buildings including calibration of the computer models are reported in Kunnath et al. (2004). Note that the simulation models of the frames used in the evaluation represent the actual state of the building and the corresponding fundamental periods are calibrated to observed response.

## GROUND MOTION DATABASE

The ground motion database compiled for NTH analyses constitutes a representative number of far-fault and near-fault ground motions from a variety of tectonic environments. A total of 21 records were selected to cover a range of frequency content, duration, and amplitude. Near-fault records were chosen so as to consider the presence of both forward-directivity and fling-step effects. Hence the assembled database can be investigated in three sub–data sets. The first set contains seven ordinary far-fault ground motions recorded within 80 km of the causative fault plane from earthquakes in the magnitude ($M_W$) range of 6.4 to 7.5 at soil or stiff soil sites. The second set includes seven near-fault ground motions characterized with forward-directivity effect. These ground motions were populated from the SAC steel project (Somerville et al. 1997b) and the CDMG Strong Motion Instrumentation Program (Somerville 1998), and contains records either taken from soil or stiff soil sites. These records are from earthquakes having a magnitude ($M_W$) range of 6.7 to 7.1, and recorded at closest fault distance of 0.0 to 15 km. In the final set, a total of seven near-fault ground motions characterized with fling-step displacement were collected. They were recorded from the 1999 ($M_W$ 7.4) Kocaeli (Turkey) and 1999 ($M_W$ 7.6) Chi-Chi (Taiwan) earthquakes at distances of 2.2 to 13.8 km. Pertinent information on the ground motion data sets including faulting mechanism, site classification of stations and peak ground acceleration (PGA), peak ground velocity (PGV), and peak ground displacement (PGD) of records are presented in Table 1. Also shown in this table is the fling displacement of near-fault records.

It is of significance to note that raw acceleration data was used for fling records of the Kocaeli and Chi-Chi earthquakes, since conventional data processing procedures eliminate or distort the original waveforms through filtering. Utilized in this study is a data processing technique proposed in Iwan et al. (1985) and refined in Iwan and Chen (1994) to recover the long period components from near-fault accelerograms, and the process has been extensively elaborated in Boore (2001) and Boore et al. (2002) during the correction of 1999 Chi-Chi and Hector Mine earthquake records, respectively. In this paper, the pre-event mean was removed using the zero-order correction described in Boore (2001) prior to the application of the baseline correction.

The major concern in baseline correction is the selection of appropriate corner periods to establish the segmental polynomial fits to satisfy two requirements: First, true tectonic deformation should be represented in the displacement time history. Second, the final velocities should oscillate around zero reference after the end of the time series.

**Table 1.** Ground motion database

| No. | Year | Earthquake | $M_W$ | Mech.[a] | Station | Comp. | Source[b] | Site Class | PGA (g) | PGV (cm/sec) | PGD (cm) | Fling Disp. (cm) |
|---|---|---|---|---|---|---|---|---|---|---|---|---|
| (*a*) *Far-Fault Recordings* | | | | | | | | | | | | |
| 1 | 1952 | Kern County | 7.5 | TH/REV | Taft | 111 | 1 | Soil | 0.18 | 17.50 | 8.79 | — |
| 2 | 1979 | Imperial Valley | 6.5 | SS | Calexico | 225 | 1 | Soil | 0.27 | 21.24 | 9.03 | — |
| 3 | 1989 | Loma Prieta | 7.0 | OB | Presidio | 00 | 1 | Soil | 0.10 | 12.91 | 4.32 | — |
| 4 | 1989 | Loma Prieta | 7.0 | OB | Cliff House | 90 | 1 | Stiff soil | 0.11 | 19.79 | 5.02 | — |
| 5 | 1992 | Big Bear | 6.4 | SS | Desert Hot Spr. | 90 | 2 | Soil | 0.23 | 19.14 | 4.53 | — |
| 6 | 1994 | Northridge | 6.7 | TH | Century CCC | 90 | 2 | Soil | 0.26 | 21.19 | 7.85 | — |
| 7 | 1999 | Kocaeli | 7.4 | SS | Ambarli | EW (90) | 1 | Soil | 0.18 | 33.23 | 25.85 | — |
| (*b*) *Near-Fault Recordings* (*Forward-Rupture Directivity*) | | | | | | | | | | | | |
| 1 | 1989 | Loma Prieta | 7.0 | OB | LGPC | 00 | 1 | Stiff soil | 0.56 | 94.81 | 41.13 | — |
| 2 | 1989 | Loma Prieta | 7.0 | OB | Lexington Dam | 90 | 1 | Stiff soil | 0.41 | 94.26 | 36.66 | — |
| 3 | 1992 | Cape Mendocino | 7.1 | TH | Petrolia | 90 | 1 | Stiff soil | 0.66 | 90.16 | 28.89 | — |
| 4 | 1992 | Erzincan | 6.7 | SS | Erzincan | EW | 1 | Soil | 0.50 | 64.32 | 21.93 | — |
| 5 | 1994 | Northridge | 6.7 | TH | Rinaldi | 275 | 2 | Soil | 0.84 | 174.79 | 48.96 | — |
| 6 | 1994 | Northridge | 6.7 | TH | Olive View | 360 | 1 | Soil | 0.84 | 130.37 | 31.72 | — |
| 7 | 1995 | Kobe | 6.9 | SS | KJMA | 00 | 1 | Stiff soil | 0.82 | 81.62 | 17.71 | — |
| (*c*) *Near-Fault Recordings* (*Fling-Step*) | | | | | | | | | | | | |
| 1 | 1999 | Kocaeli | 7.4 | SS | Sakarya (SKR) | EW | 3 | Stiff soil | 0.41 | 82.05 | 205.93 | 186.76 |
| 2 | 1999 | Kocaeli | 7.4 | SS | Yarimca (YPT) | NS | 3 | Soil | 0.23 | 88.83 | 184.84 | 145.79 |
| 3 | 1999 | Chi-Chi | 7.6 | TH | TCU052 | NS | 4 | Soil | 0.44 | 216.00 | 709.09 | 697.12 |
| 4 | 1999 | Chi-Chi | 7.6 | TH | TCU068 | EW | 4 | Soil | 0.50 | 277.56 | 715.82 | 601.84 |
| 5 | 1999 | Chi-Chi | 7.6 | TH | TCU074 | EW | 4 | Soil | 0.59 | 68.90 | 193.22 | 174.56 |
| 6 | 1999 | Chi-Chi | 7.6 | TH | TCU084 | NS | 4 | Soil | 0.42 | 42.63 | 64.91 | 59.43 |
| 7 | 1999 | Chi-Chi | 7.6 | TH | TCU129 | NS | 4 | Soil | 0.61 | 54.56 | 82.70 | 67.54 |

[a] Faulting Mechanism=TH: Thrust; REV: Reverse; SS: Strike-slip; OB: Oblique

[b] Data Source=1: PEER (http://peer.berkeley.edu/smcat); 2: Cosmos (http://db.cosmos-eq.org); 3: ERD (http://angora.deprem.gov.tr/); 4: http://scman.cwb.gov.tw/eqv5/special/19990921/pgadata-asci0704.htm

Note: Original fling ground motions from data source (3) and (4) were reprocessed.

The residual displacement due to fling step were computed based on the GPS measurements for Chi-Chi earthquake ground motions; this information was retrieved from the study by Boore (2001). Since such reported information is not available for Kocaeli earthquake stations, the baseline corrections of the Kocaeli records were only performed considering the requirement of the zero-velocity crossing at the end of the time history. The purpose of applying such a correction procedure in this study is to get consistency in fling records reflecting the true permanent ground displacement, thus to investigate consequences of static offset in the displacement time history on structural response. Studies (Boore et al. 1999, Boore 2001) have shown that elastic response spectra for periods less than about 20 sec are usually not affected by the baseline correction.

## RESPONSE SPECTRA OF GROUND MOTIONS

For NTH analyses presented in subsequent sections, ground motions given in Table 1 were scaled such that the spectrum of each record matches the 5 percent damped *UBC* (ICBO 1997) design spectrum with minimum error in the period range of 0.6 sec to 4.0 sec. Hence the mean of the seven records in each ground motion category reasonably represent the design spectrum. Such a scaling procedure has been used previously (Alavi and Krawinkler 2004) and found to be necessary to facilitate the comparison of results from the different ground motion sets in a consistent manner. Design spectrum parameters were selected so as to consider explicitly the near-fault effects via near-source amplification factors ($N_A$ and $N_V$) introduced in *UBC*. Therefore the spectrum was constructed for soil type $S_D$ and fault distance of 5 km (Seismic Zone 4). The spectra of the scaled ground motions together with the design spectrum are presented in Figure 5. Also marked on this figure are the fundamental periods of each building (Figure 5c). The fundamental modal periods for the buildings are as follows: 4-story building, $T_1 = 1.05$ sec; 6-story building, $T_1 = 1.40$ sec; and 13-story building, $T_1 = 3.05$ sec. It is observed that for near-fault motions, particularly for fling records, the effect of the inherent pulse tends to increase the long-period portion of the acceleration response spectrum (Figures 5a and 5b). This suggests that amplifying the design spectrum with explicit near-source factors as in *UBC* may not be always conservative.

## SEISMIC RESPONSE EVALUATION OF BUILDINGS

In all, 63 nonlinear time-history (NTH) simulations were conducted on the three buildings. Interstory drift ratio (IDR), defined as the relative displacement between two consecutive story levels normalized by the story height, is used as the primary measure of seismic demand. Additional demand measures, such as component and story ductility were also investigated. In general there is reasonable correlation between interstory drift demands and component/story-level ductility demands; hence these results are not included here. The peak interstory drift profiles obtained from NTH analyses of the buildings subjected to the three sets of ground motions (i.e., far-fault motions, near-fault motions with forward directivity, and near-fault motions with fling step) are presented in Figure 6 with their associated dispersion values. For the 4-story building, far-fault motions produce nearly uniform interstory drift demands for most records, with the exception of the Taft record, which triggers higher-mode effects resulting in increased de-

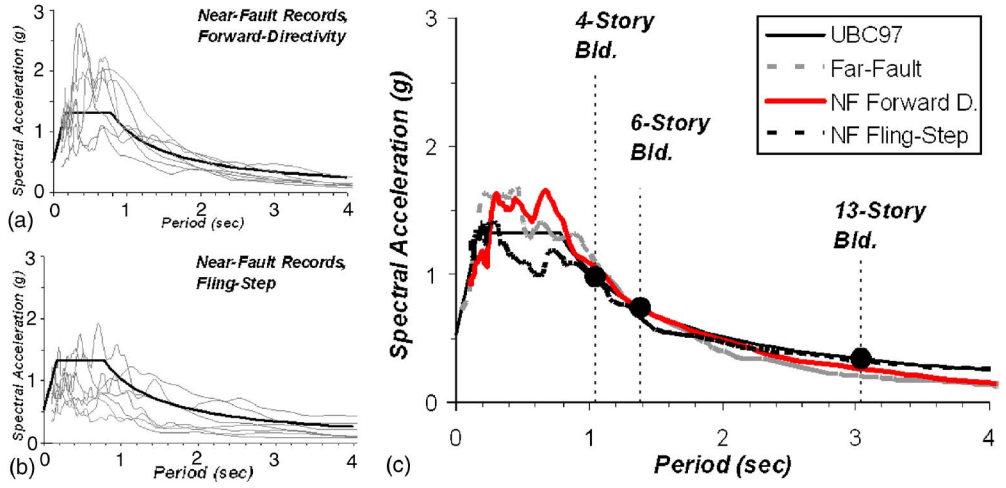


**Figure 5.** *UBC* (ICBO 1997) design spectrum and response spectra of (a) original forward-directivity records, (b) original fling-step records, and (c) design spectrum and mean response spectra of scaled ground motions. (Note: dashed lines indicate the fundamental period of each building.)

mands in the upper stories. In case of near-fault records, they impose higher demands than far-fault records though the maximum drift is generally concentrated at the lower story levels. The largest demand is caused by the Chi-Chi record (TCU052), which produced a 3.6 percent interstory drift at the first story.

For the 6-story building, the maximum story demand for far-fault records is observed to be either at the first or fifth story levels and depends on the frequency content of the motion. Though similar observations hold for near-source records, the demands at the intermediate levels are much higher. Of the entire data set, the SKR record generated the highest demand (5.3 percent interstory drift) at the first story. Three near-fault ground motions in particular (Rinaldi, Erzincan, and TCU068) created significant demands at intermediate stories. For the 13-story building, the SKR record (a typical near-fault motion with fling step) generated the highest demand (5 percent interstory drift) at the second story level. Higher-mode effects are predominant in many of the near-fault records (e.g., YPT, TCU0129, Olive V., Rinaldi) causing a shift in demands from the lower to upper stories. The variation in story demand for the far-fault records is less significant.

While higher-mode effects are expected to contribute to the response of the 6- and 13-story buildings, the response of the 4-story building demonstrates that even for low-rise buildings, higher-mode effects could play a role. In order to ascertain the contribution of higher modes, it was necessary to inspect both the acceleration and velocity spectra of the ground motions collectively. Figure 7 depicts the spectral velocity of the critical records that generated the largest demands in the three buildings. In examining

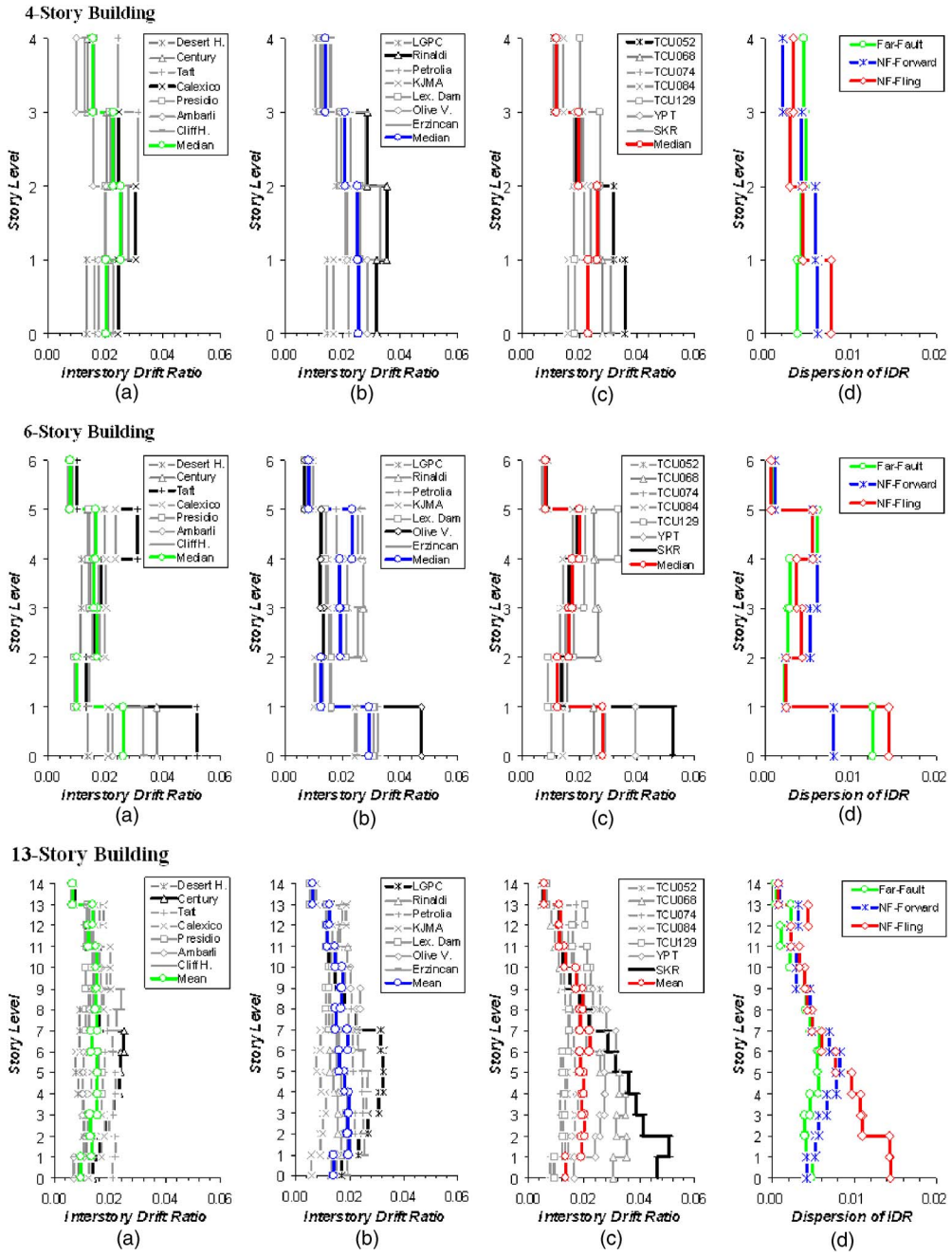


**Figure 6.** Maximum interstory drift for each building subjected to spectrum-compatible (a) far-fault motions, (b) near-fault motions with forward directivity, (c) near-fault motions with fling step, and (d) dispersion of interstory drift ratio (IDR).

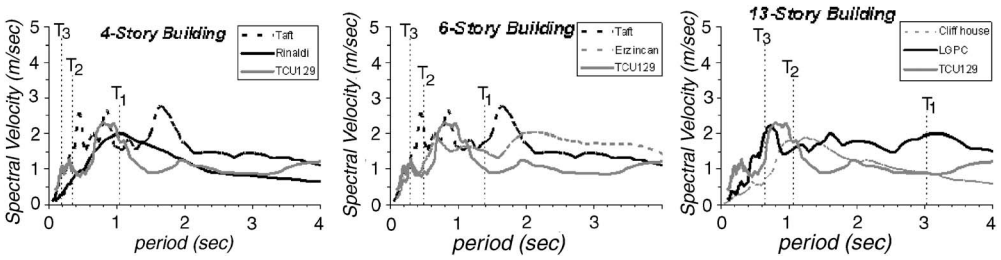


**Figure 7.** Velocity spectra of selected ground motions.

the spectral content of records, it must be noted that modal periods are constantly changing in a nonlinear system and that so-called higher-mode periods also shift as the building moves into the inelastic range. The dashed lines shown in Figure 7 refer to the modal periods in the elastic range. All these lines will gradually move to the right as component yielding progresses. For the objective of correlating the information on the spectral demands with the observed behavior, the building responses were re-examined. Therefore, for the 4-story building, though most of the records caused higher demands in the lower stories, Taft and TCU129 records are seen to activate higher-mode effects resulting in increased demands in the upper and intermediate stories. The spectral velocities at the second and third modes for the Taft and TCU129 records are more significant than their first-mode counterpart. Yet for the Rinaldi record, the dominant first-mode response is clearly observed from the velocity spectra. Similarly, looking at the velocity spectra for the Taft, Erzincan, and TCU129 records explains the observed higher-mode response for the 6-story building. Finally, for the 13-story building, Cliff house, LGPC, and TCU129 motions produced larger demands at intermediate and upper levels. The spectral velocities for these records at the higher-mode periods are much larger than that for the fundamental period, keeping in mind that a shift to the right of the spectra is to be expected as yielding of components occur.

In summary, the median maximum demands as well as the scatter (dispersion) in the peak values for the three buildings were higher for near-fault records than far-fault motions. Additionally, the demands in the lower levels for records with fling step were significantly higher than records with forward-directivity. Overall, higher-mode effects were more predominant in forward-directivity records. In Figure 8, the severity of near-fault ground motions having forward directivity and fling step are compared with far-fault motions at the component level. $M/M_y$ is the ratio of the moment demand to the yield moment, and $\theta/\theta_y$ is the ratio of the member end rotation to the yield rotation. The results shown are for a typical element but they convey the general difference in component demands between far-fault and near-fault ground motions. In this case, the demands on an interior column on the first-story level of the 6-story building experiencing the largest demand among each ground motion category are presented.

The largest deformation demands in near-fault shaking are associated with fewer reversed cycles of loading. This effect is due to the presence of long-duration high-

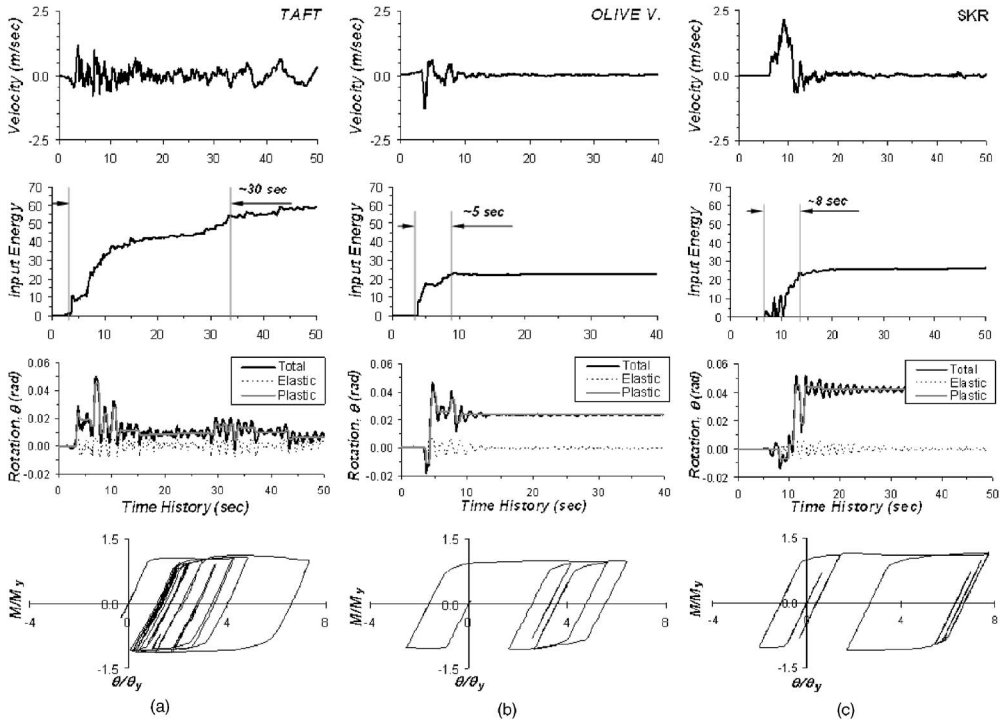


**Figure 8.** Cyclic demand for a typical column subjected to (a) far-fault motion (Taft), (b) near-fault motion with forward directivity (Olive V.), and (c) near-fault motion with fling step (SKR).

amplitude pulses in near-fault records, causing dissipation of sudden energy in a short period of time in a single or few excursions. On the other hand, the energy demand on a structural system subjected to a far-fault motion tends to gradually increase over a longer duration, causing an incremental build-up of input energy. The total input energy variation for each record is also displayed in Figure 8. It can be inferred from the figure that the magnitude of the input energy by itself is not a complete measure of the severity of the ground motion. For example, the peak demands can be caused by ground motions with smaller input energies. Another important observation that was alluded to earlier is the fact that the gradual build up of input energy for far-fault records results in increased reversed inelastic cyclic action and low-cycle fatigue damage, while near-fault motions are characterized by fewer inelastic displacement cycles followed by several cycles of elastic action. The consequence of a single predominant peak is a well-pronounced permanent offset (displacement), and the subsequent response is essentially a series of elastic cycles about this deformed configuration. Also shown in Figure 8 are the inelastic and elastic components of the total deformation. It is evident that the elastic part of the rotation is almost negligible, which suggests that for ductile elements with significant inelastic behavior, the peak component deformation is generally equivalent to the plastic deformation.

Figure 8 also provides a glimpse of the implications of cyclic demand and the influence of low-cycle fatigue on the performance of structures. The ductility demands on the column are 7.6, 6.4, and 7.7 for the Taft, Olive V., and SKR records, respectively. However, there are numerous additional cycles of deformation that exceed the yield rotation for the far-fault motion. Since the inelastic response results in a permanent drift, it is more convenient to count the number of half-cycles wherein each half-cycle is the peak-to-peak amplitude. If the peak-to-peak amplitude exceeds twice the yield rotation, each such cycle is referred to as a "plastic cycle." For the critical column shown in Figure 8, there were 20 half-plastic cycles during the response to the far-fault record. The near-fault motions with forward-directivity (Olive V) and fling-step effects (SKR) both resulted in only 6 half plastic cycles. The cumulative damage resulting from plastic cycles is much greater than implied by the peak ductility demand, and should not be ignored when assessing the performance of the component (Kunnath and Kalkan 2004).

From the preliminary information generated through the evaluation of the three buildings discussed above, it is clear that buildings respond differently to far-fault and near-fault ground motions. However, in order to achieve a more coherent understanding of the effects of near-fault records, a systematic study was conducted on the same structures using simple pulse motions that reasonably represent forward-directivity and fling effects.

## SIMPLE MATHEMATICAL MODELS FOR NEAR-FAULT GROUND MOTION PULSES

Simple pulses do not necessarily match the ground acceleration of original records (Makris and Chang 2000). It would also be unrealistic to expect that near-fault records can be represented fully by equivalent simple pulses. Since near-fault recordings come from great variations in the vicinity of an active fault system, the wave propagation pattern of ground motion is strongly affected by radiation pattern, directivity, rupture mechanism, stress drop, and also by geomorphology and lateral scatter; therefore, real recordings may contain high-frequency components as well as several nonhomogeneous velocity peaks. Based on the complex form of near-fault records, it is not always possible to calibrate simple models to satisfy all conditions aforementioned unless the real record to be represented is significantly simple. For the representation of near-fault records one can utilize more complicated pulse models such as those derived based on wavelet functions (e.g., Mavroeidis and Papageorgiou 2003, Mavroeidis et al. 2004); however, they still have similar limitations, and their calibration is even more difficult due to the presence of supplementary parameters in the definition of wavelet functions. Despite the stated limitations, the use of simple pulses offers a distinct advantage in distinguishing the response of typical structures to variations in pulse characteristics.

Recent studies by Sasani and Bertero (2000) and Alavi and Krawinkler (2004) have demonstrated that simple pulses can be used to capture the salient response characteristics of structures subjected to near-fault ground motions within limitations. In the following, near-fault pulse-type motions are simulated using waveforms that approximately reproduce the response spectrum of actual near-fault records as a function of time-domain parameters such as the duration and amplitude of the near-fault pulse. Two types

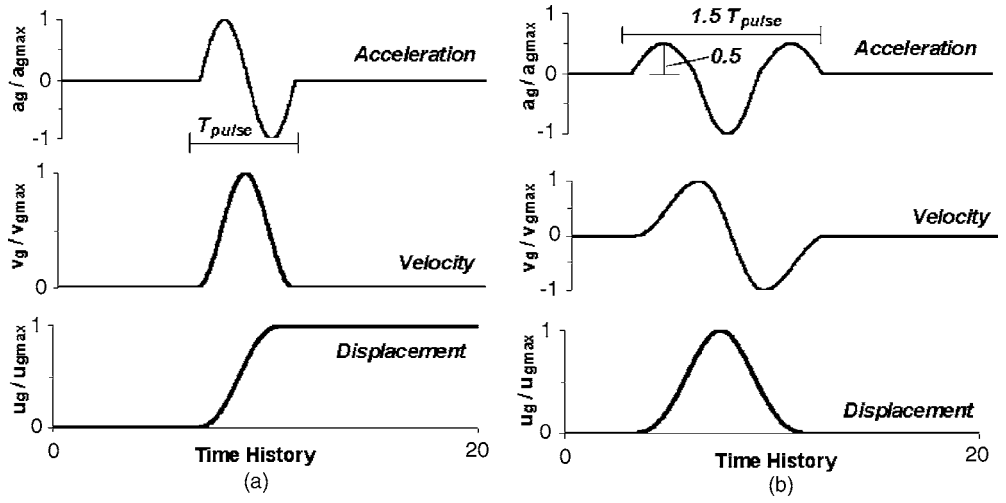


**Figure 9.** Idealized sinusoidal pulses: (a) fling-step (Type A), (b) forward-directivity (Type B). (Note: curves are normalized by maximum acceleration, velocity, and displacement.)

of sinusoidal wave shapes previously studied by Sasani and Bertero (2000) were used to mimic near-fault records having forward-directivity and fling-step displacement. Simplified waveform representations are defined by the number of half cycles as shown in Figure 9. Figure 9a approximates a fling-step type of motion where the record exhibits a static offset at the end of the displacement time history, while Figure 9b represents a forward-directivity-type of motion.

The mathematical models for the acceleration time history of the two pulse models can be expressed as follows:

- Pulse Type A (Fling-step)

$$a(t) = \frac{2\pi D}{T_p^2} \sin\left[\frac{2\pi}{T_p}(T - T_i)\right] \tag{1}$$

- Pulse Type B (Forward-directivity)

$$a(t) = \frac{2\pi D}{T_p^2} \sin\left[\frac{2\pi}{T_p}(T - T_i)\right] \quad \text{for} \begin{cases} Ti < T < (Ti + 0.5Tp) \\ (T_i + T_p) < T < (T_i + 1.5T_p) \end{cases} \tag{2}$$

$$a(t) = \frac{2\pi D}{T_p^2} \sin\left[\frac{2\pi}{T_p}(T - T_i)\right] \quad \text{for } (Ti + 0.5Tp) < T < (Ti + Tp) \tag{3}$$

where $D$ is the maximum amplitude of the displacement obtained by double time-integration of acceleration, a(t), $T_p$ is the period of sin-pulse, and $T_i$ is the pulse arrival time. The acceleration, velocity, and displacement (5 percent damped) elastic response spectra of the pulse models are shown in Figure 10 where the spectral ordinates are nor-

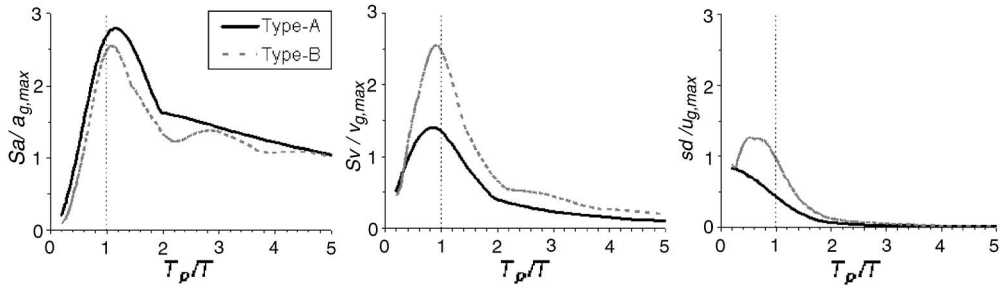


**Figure 10.** Five percent damped normalized (a) acceleration, (b) velocity, and (c) displacement response (elastic) spectra for idealized sinusoidal pulses. (Type A: fling-step; Type B: forward-directivity.)

malized by their corresponding peak time-history values (i.e., PGA, PGV, and PGD). It should be noted that for a given pulse intensity ($a_{g,\max}$) for both pulse models, PGV for Type B pulse, used to normalize the velocity spectrum, is half of that for Type A pulse; similarly for the normalization of the displacement spectrum, the ratio of PGD of pulse Type B to that of Type A is around 0.25. Yet it is evident from the velocity and displacement spectra that a Type B pulse is more damaging than a Type A pulse. Although it is obvious for simple pulse models that the predominant period of motion coincides approximately with the peak of velocity response spectrum, it is not always possible to capture the pulse period of actual near-fault records as easily and accurately due to the presence of multiple peaks in the velocity spectrum.

## RESPONSE OF BUILDINGS TO SIMPLE PULSE MODELS

The building models are re-analyzed using simple pulse models with forward-directivity and fling-step effects to study the influence of pulse period on interstory drift demands. In this parametric study, the pulse period is varied from 0.5 to 1.5 of the fundamental period of the buildings. Prior to application of the pulses, pulse records were scaled in a manner consistent with the ground motion scaling procedure whereby the acceleration spectra of each pulse matched the 5 percent damped *UBC* design spectrum with minimum dispersion in the period range of 0.6 sec to 4.0 sec by adjusting the pulse intensity. This was necessary to enable a reasonable comparison to the results obtained in the previous phase of the study. Figures 11–13 summarize the responses of 4-, 6-, and 13-story buildings to ground motion inputs characterized by both pulse types A and B. The roof drift indicated in the plots are the ratio of the roof displacement to the building height.

The distributions of response parameters collectively confirm that demand is conditioned on the ratio of pulse period ($T_p$) to fundamental period ($T$). Demands are clearly amplified as the pulse period approaches the fundamental period of the building model. In the neighborhood where $T_p/T = 1.0$, the maximum story demands are concentrated on the lower levels indicating a primarily first-mode response. This holds true even as the

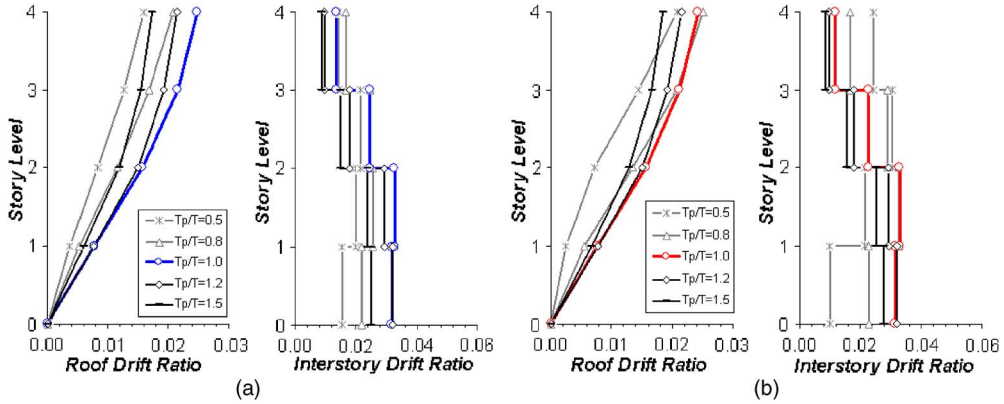


**Figure 11.** Dependence of roof drift ratio and interstory drift ratio on $T_p/T$ for 4-story building subjected to idealized pulses (a) Type A, and (b) Type B.

ratio $T_p/T$ exceeds unity. When the ratio is much lower than 1.0 and the pulse period approaches the second and third modal periods, the maximum interstory demands migrate to the upper stories, clearly identifying the contributions of higher modes. Similar findings have been reported in Alavi and Krawinkler (2004) where MDOF generic frames were subjected to forward-directivity–type pulses with various $T_p/T$ values.

Observations synthesized from Figures 11–13 indicate that forward-directivity pulses result in higher demands than fling-step pulses. This can be attributed to the forward and backward momentum acquired during the initial and final phase of the forward-directivity pulse. On the other hand, fling type of motion contains only forward momentum. In the case of forward directivity, the maximum drift demand in the upper

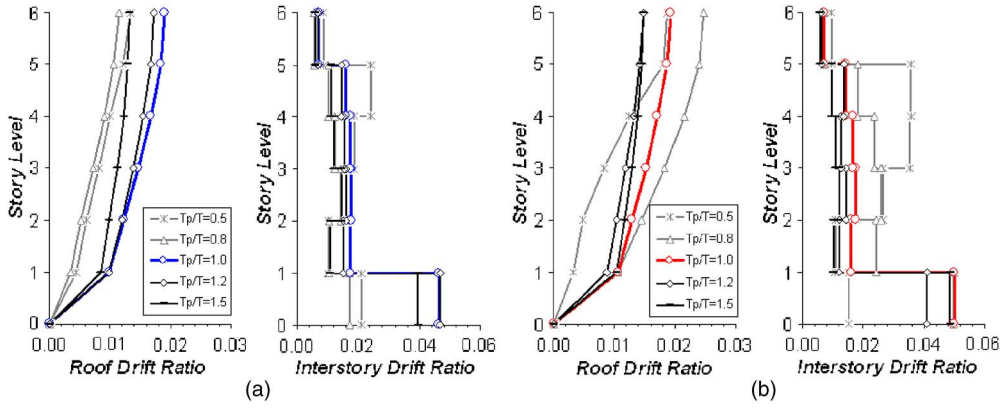


**Figure 12.** Dependence of roof drift ratio and interstory drift ratio on $T_p/T$ for 6-story building subjected to idealized pulses (a) Type A, and (b) Type B.

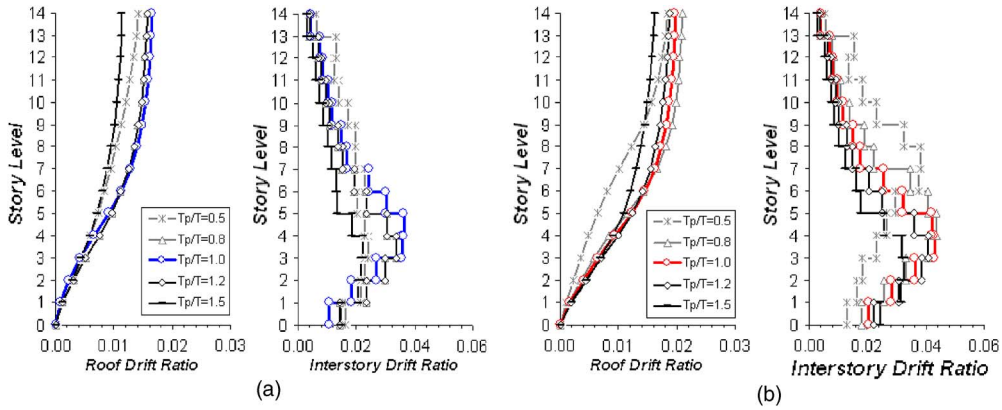


**Figure 13.** Dependence of roof drift ratio and interstory drift ratio on $T_p/T$ for 13-story building subjected to idealized pulses (a) Type A, and (b) Type B.

stories in many cases is almost two times higher than that produced by fling motions. Higher-mode effects are not as evident in the response to fling-type motions, but are more clearly evident in all buildings for forward-directivity pulses when $T_p/T$ is less than 0.8.

Additional insight on the transient response at the story and component levels for each pulse type is demonstrated in Figure 14. Shown in the figure are the third-story interstory drift variation and interior column base rotation from the 13-story building. The pulse period is equal to the fundamental period of the building for both cases. The analyses indicate that, upon arrival of the pulse, the building starts to deform and is eventually displaced into the inelastic range in the same cycle. The peak time and end time of each pulse are indicated in the figure by dash lines. Following the impact of pulse Type B, the third story displaces laterally by 40 mm, which corresponds to 3.8 percent interstory drift. For reference, the elastic drift limit in the third story is 0.7 percent. Initially two pulses follow the same path dictated by the forward momentum phase, but the reversing phase of pulse Type B increases the response compared to pulse Type A. The higher peak-to-peak amplitude of the reversing pulse represented by pulse Type B has greater damage potential particularly if the pulse period is close to the fundamental period of the building.

## EFFECTS OF INCORPORATING ARTIFICIAL FLING EFFECT ON NEAR-FAULT GROUND MOTIONS HAVING FORWARD DIRECTIVITY

The results presented in preceding sections suggest that fling effects are less significant than forward directivity and that systems subjected to records with predominant fling-step displacements respond primarily in the first mode. To further investigate the consequences of fling-step effects, a final series of simulations was carried out in which actual records with forward directivity were modified to include fling-step displacement. As indicated earlier, this coupling is unlikely, given that fling step occurs in the direction

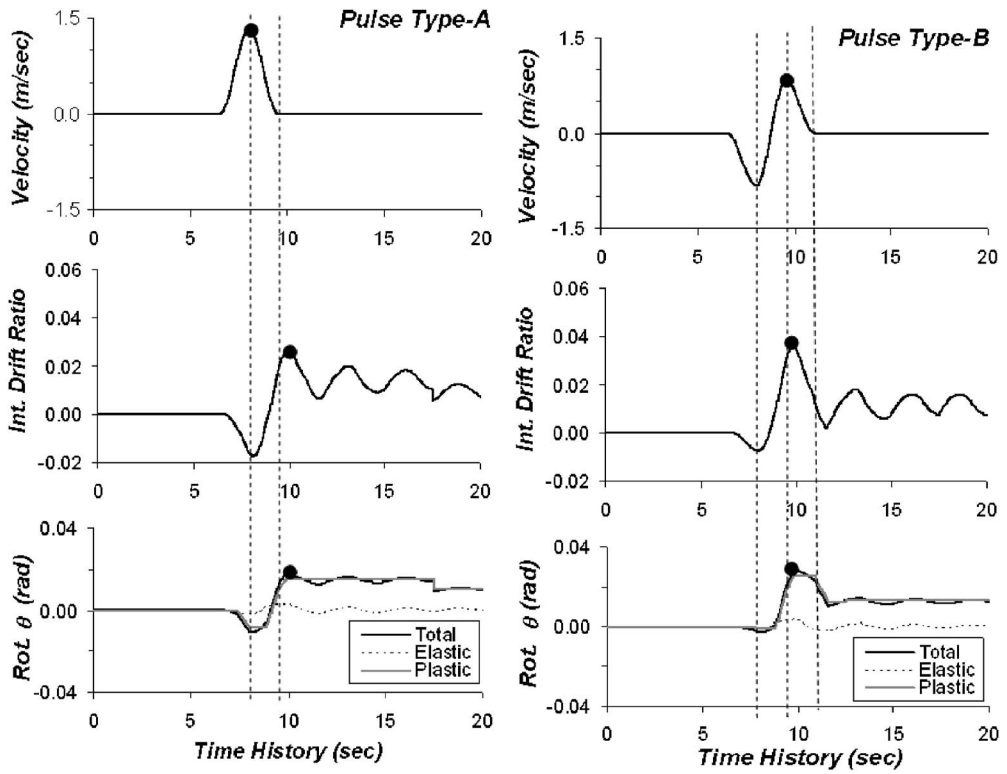


**Figure 14.** Interstory drift variation at critical (third) story level and rotation time history of interior column experiencing maximum demands at same story level of the 13-story building subjected to pulse Types A and B. (Note: dashed lines denote the time at peak magnitude and the end time of pulses.)

of fault slip while forward directivity is associated in the fault-normal direction as in strike-slip faults. However, this theoretical study will serve to provide an understanding of the severity of fling-step displacements and offer a conservative approximation of near-fault effects in seismic evaluation.

The artificial fling motion is generated by incorporating Type A velocity pulse into near-fault records that are originally characterized by forward directivity only. The contribution from the pulse motion to the simulated ground motion (i.e., static offset in the displacement time history) is manipulated by changing the velocity amplitude of the pulse model. The arrival of the peak velocity (in Type A) is adjusted to occur at approximately the same time as the peak velocity of the original ground motion. The pulse period is selected to match the building period. The amplitude of the pulse is carefully selected so as not to distort the intensity of the original motion, but rather to introduce fling effects. The sequence of the procedure to create an artificial fling-step displacement is presented for the 13-story building in Figure 15. One of the records from the Rinaldi

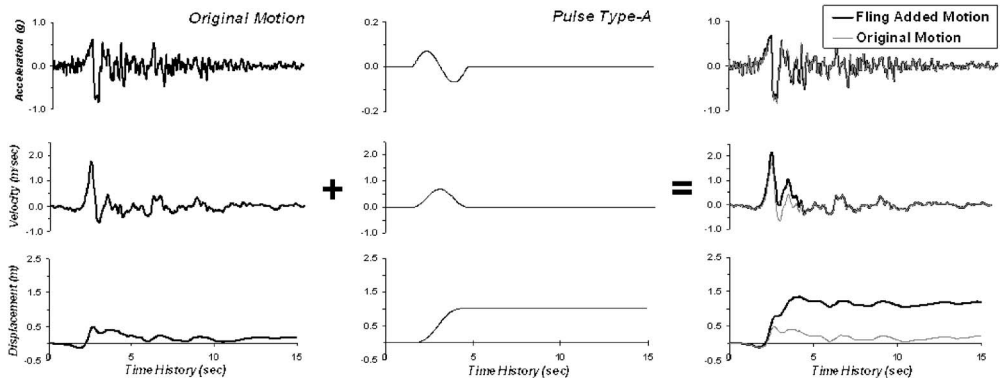


**Figure 15.** Sequence of generating an artificial fling effect using original Rinaldi record and pulse Type A. (Note: $T_p$ of pulse Type A = fundamental period of target building.)

station during the 1994 Northridge, California, earthquake is selected for illustration. Also shown in this figure are the acceleration, velocity, and displacement histories of the original and modified motions.

The pulse periods of the fling motions added to the Rinaldi records were based on the fundamental periods of each building, and therefore for each building a new record was generated. Figure 16 shows the fast Fourier amplitude spectrum of the original and

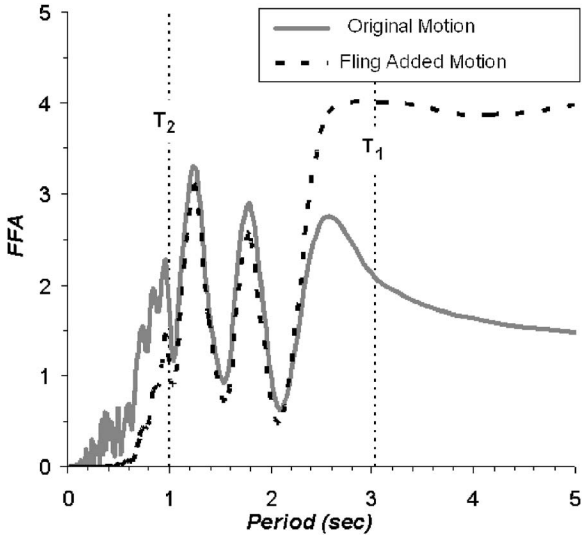


**Figure 16.** Comparison of fast Fourier amplitude of original and unscaled fling-added motion ($T_1$ and $T_2$ denote the first and second fundamental period of 13-story building).

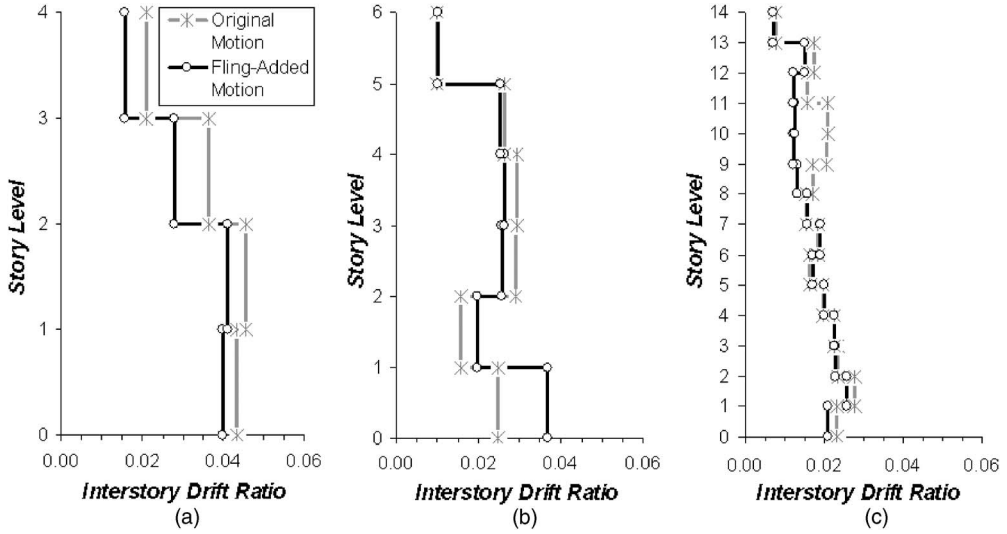


**Figure 17.** Comparison of response of (a) 4-story, (b) 6-story, and (c) 13-story buildings to original and fling-added motion.

fling-added motion. It is observed that the spectral shapes are generally preserved with small amplitude changes in the spectral demands at periods between 1.0 sec to 2.5 sec. Conversely, the addition of fling amplified the first-mode spectral amplitude, however, it reduced the spectral amplitudes at periods less than 1.0 sec. The consequence of this alteration is to further excite the fundamental mode while suppressing the contribution of the higher modes. This effect is clearly evident in the response of the three buildings shown in Figure 17. The original records containing forward directivity clearly show the influence of higher modes with significant interstory demands in the upper stories. When the fling-modified motions are applied to the frames, the demands in the upper stories are visibly reduced, indicating a suppression of higher-mode effects. It should be noted that similar scaling procedure as described before is applied to fling-added motions prior to NTH analyses.

## SUMMARY AND CONCLUSIONS

Although observed damage and failure of engineered structures during recent earthquakes have revealed the susceptibility of the existing building stock to near-fault ground motions, there is still considerable uncertainty on the consequences of near-fault ground motions on the response of typical building structures. Current practice is not adequately equipped to incorporate the effects of coherent long-period pulses in thedesign process. Methods to implicitly consider inelastic demands by amplifying the design spectra do not provide a reliable basis for representing near-fault ground motions. Hence the purpose of this study is to provide new insight and additional data on the response of moment frames to near-fault ground motions, and to contrast the demands with far-fault records.

The analytical simulations carried out in this study show that typical steel moment frames can be subjected to large displacement demands at the arrival of the velocity pulse that require the structure to dissipate considerable input energy in a single or relatively few plastic cycles. This demand will impact structures with limited ductility capacity. In contrast, far-fault motions build input energy more gradually, and though the displacement demands are on average lower than the demands in near-fault records, the structural system is subjected to significantly more plastic cycles. Hence cumulative effects are more pronounced in far-fault ground motions. This finding is significant in the development of testing protocols and damage models incorporating low-cycle fatigue (El-Bahy et al. 1999a, b).

Studies with simple pulses clearly demonstrated the migration of demands from lower to upper stories when the ratio of the pulse period to building period was below 0.8. Records with forward directivity resulted in more instances of higher-mode demand while records with fling-step displacement almost always caused the systems to respond primarily in the fundamental mode. For all the near-fault pulses investigated in this study, the severity of the demands is controlled by the ratio of the pulse to system period.

It has long been recognized that near-fault motions characterized by forward-directivity effects are potentially more damaging, but the consequences of fling-step displacements have not been as well understood. In the present study, fling effects were considered in several ways: by examining the response of buildings to recorded ground motions that contain fling effects, by using equivalent half-sinusoidal pulses, and by artificially introducing carefully calibrated pulses into actual near-fault recordings. Although simple-pulse waveforms do not contain all the characteristics of recordings from real earthquakes, they provide a convenient means of understanding and correlating the relationship between pulse periods, system characteristics, and inelastic demands. Findings from this study indicate that near-fault records with fling can be more damaging than far-fault records but they tend to accentuate first-mode behavior.

Finally, it can also be concluded that a careful examination of acceleration and velocity spectra collectively can provide engineers with a reasonable assessment of the damage potential of near-fault records. Demands in the fundamental and higher modes must be evaluated by taking into consideration the fact that modal periods shift to the right of the spectrum as the system moves from the elastic to inelastic state.

The present study was limited to typical existing steel-frame buildings with fully rigid connections. Stable hysteretic behavior was assumed in the nonlinear simulations without consideration of component deterioration or potential weld fracture. Incorporating such effects will shed light on additional issues, but the general findings reported in this study are expected to remain valid for regular moment-frame buildings with stable force-deformation behavior. Finally, other ground motion parameters such as intensity of the record and structural system parameters such as plan and vertical irregularities are also expected to play a role in the imposed seismic demands, and need to be investigated systematically in order to arrive at a complete understanding of the effects of near-fault records on building structures.

## ACKNOWLEDGMENTS

Funding for this study provided by the National Science Foundation under Grant CMS-0296210, as part of the U.S.-Japan Cooperative Program on Urban Earthquake Disaster Mitigation, is gratefully acknowledged. Any opinions, findings, and conclusions or recommendations expressed in this material are those of the authors, and do not necessarily reflect the views of the National Science Foundation.

## REFERENCES

Abrahamson, N., 2001. Incorporating Effects of Near Fault Tectonic Deformation into Design Ground Motions, a presentation sponsored by the Earthquake Engineering Research Institute Visiting Professional Program, hosted by the State University of New York at Buffalo, 26 Oct. 2001. Available at http://mceer.buffalo.edu/outreach/pr/abrahamson.asp

Alavi, B., and Krawinkler, H., 2004. Behaviour of moment resisting frame structures subjected to near-fault ground motions, *Earthquake Eng. Struct. Dyn.* **33**, 687–706.

American Society of Civil Engineers (ASCE), 2000. *Prestandard and Commentary for the Seismic Rehabilitation of Buildings*, prepared for the SAC Joint Venture, published by the Federal Emergency Management Agency, *FEMA-356*, Washington D.C.

Applied Technology Council (ATC), 1996. *Seismic Evaluation and Retrofit of Concrete Buildings*, Volumes 1 and 2, *Report No*. *ATC-40*, Redwood City, CA.

Boore, D., 2001. Effect of baseline correction on displacements and response spectra for several recordings of the 1999 Chi-Chi, Taiwan, earthquake, *Bull. Seismol. Soc. Am.* **91** (5), 1199–1211.

Boore, D., Stephens, C. D., and Joyner, W. B., 2002. Comments on baseline correction of digital strong motion data: Examples from the 1999 Hector Mine California earthquake, *Bull. Seismol. Soc. Am.* **92** (4), 1543–1560.

El-Bahy, A., Kunnath, S. K., Stone, W. C., and Taylor, A. W., 1999a. Cumulative seismic damage of circular bridge columns: Benchmark and low-cycle fatigue tests, *ACI Struct. J.* **96** (4), 633–641

——— 1999b. Cumulative seismic damage of circular bridge columns: Variable amplitude tests, *ACI Struct. J.* **96** (5), 711–719.

Galesorkhi, R., and Gouchon, J., 2000. Near-source effects and correlation to recent recorded data, *Proceedings, 6th U.S. National Conference on Earthquake Engineering, Seattle, Wash.*

International Conference of Building Officials (ICBO), 1973. *Uniform Building Code*, Whittier, CA.

——— 1988. *Uniform Building Code*, Whittier, CA.

——— 1997. *Uniform Building Code*, Whittier, CA.

——— 2000. *International Building Code*, Whittier, CA.

Iwan, W. D., Moser, M. A., and Peng, C. Y., 1985. Some observations on strong-motion earthquake measurements using a digital accelerograph, *Bull. Seismol. Soc. Am.* **75**, 1225–1246.

Iwan, W. D., and Chen, X. D., 1994. Important near-field ground motion data from the Landers earthquake, *Proceedings, 10th European Conference on Earthquake Engineering, Vienna, Austria, Aug. 28–Sept. 2*.

Hall, J. F., Heaton, T. H., Halling, M. W., and Wald, D. J., 1995. Near-source ground motions and its effects on flexible buildings, *Earthquake Spectra* **11** (4), 569–605.

Heaton, T. H., Hall, J. F., Wald, D. J., and Halling, M. W., 1995. Response of high-rise and base-isolated buildings to a hypothetical Mw 7.0 blind thrust earthquake, *Science* **267** (13), 206–211.

Kalkan, E., Adalier, K., and Pamuk, A., 2004. Near field effects and engineering implications of recent earthquakes in Turkey, *Proceedings, 5th International Conference on Case Histories in Geotechnical Engineering, New York, NY, April 13–17*, Paper No. 3-30.

Krawinkler, H., and Al-Ali, A., 1996. Seismic demand evaluation for a 4-story steel frame structure damaged in the Northridge earthquake, *Struct. Des. Tall Build.* **5** (1), 1–27.

Kunnath, S. K., and Kalkan, E., 2004. Evaluation of seismic deformation demands using nonlinear procedures in multistory steel and concrete moment frames, *ISET, Journal of Earthquake Technology*, Special Issue on Performance Based Design, **41** (1), 159–182.

Kunnath, S. K., Nghiem, Q., and El-Tawil, S., 2004. Modeling and response prediction in performance-based seismic evaluation: case studies of instrumented steel moment-frame buildings, *Earthquake Spectra* **20** (3), 883–915.

Makris, N., and Chang, S., 2000. Effect of viscous, viscoplastic and friction damping on the response of seismic isolated structures, *Earthquake Eng. Struct. Dyn.* **29**, 85–107.

Manfredi, G., Polese, M., and Cozenza, E., 2000. Cyclic demand in the near-fault area, *Proceedings, 6th U.S. National Conference on Earthquake Engineering, Seattle, Wash.*

Mavroeidis, G. P., and Papageorgiou, A. S., 2003. A mathematical expression of near-fault ground motions, *Bull. Seismol. Soc. Am.* **93** (3), 1099–1131.

Mavroeidis, G. P., Dong, G., and Papageorgiou, A. S., 2004. Near-fault ground motions, and the response of elastic and inelastic single-degree-freedom (SDOF) systems, *Earthquake Eng. Struct. Dyn.* **33**, 1023–1049.

OpenSees, 2005. Open system for earthquake engineering simulation. http://opensees.berkeley.edu

Sasani, M., and Bertero, V. V., 2000. Importance of severe pulse-type ground motions in performance-based engineering: historical and critical review, *Proceedings, 12th World Conference on Earthquake Engineering*, Paper No. 1302.

Somerville, P. G., 1998. Development of an improved representation of near-fault ground motions, *SMIP98 Proceedings, Seminar on Utilization of Strong-Motion Data, Oakland, CA, Sept. 15*, California Division of Mines and Geology, Sacramento, CA, pp. 1–20.

Somerville, P., Smith, N., Graves, R., and Abrahamson, N., 1997a. Modification of empirical strong motion attenuation relations to include the amplitude and duration effects of rupture directivity, *Seismol. Res. Lett.* **68**, 180–203.

Somerville, P., Smith, N., Punyamurthula, S., and Sun., J., 1997b. *Development of Ground Motion Time Histories for Phase 2 of the FEMA/SAC Steel Project*, prepared for the SAC Joint Venture, published by the Structural Engineers Association of California, *Report No*. *SAC/BD-97/04*, Sacramento, CA.

Uang, C. M., Yu, Q. S., Sadre, A., Youseff, N., and Vinkler, J., 1997. Seismic response of an instrumented 13-story steel frame building damaged in the 1994 Northridge earthquake, *Earthquake Spectra* **13** (1), 131–149.

(Received 30 July 2004; accepted 10 June 2005)